

Non-equilibrium transport through a disordered molecular nanowire

P. Thiessen,¹ E. Díaz,^{1,*} R. A. Römer,² and F. Domínguez-Adame^{1,2}

¹*GISC, Departamento de Física de Materiales, Universidad Complutense, E-28040 Madrid, Spain*

²*Department of Physics and Centre for Scientific Computing, University of Warwick, Coventry, CV4 7AL, United Kingdom*

We investigate the non-equilibrium transport properties of a disordered molecular nanowire. The nanowire is regarded as a quasi-one-dimensional organic crystal composed of self-assembled molecules. One orbital and a single *random* energy are assigned to each molecule while the inter-molecular coupling does not fluctuate. Consequently, electronic states are expected to be spatially localized. We consider the regime of strong localization, namely, the localization length is smaller than the length of the molecular wire. Electron-vibron interaction, taking place in each single molecule, is also taken into account. We investigate the interplay between disorder and electron-vibron interaction in response to either an applied electric bias or a temperature gradient. To this end, we calculate the electric and heat currents when the nanowire is connected to leads, using the Keldysh non-equilibrium Green's function formalism. At intermediate temperature, scattering by disorder dominates both charge and heat transport. We find that the electron-vibron interaction enhances the effect of the disorder on the transport properties due to the exponential suppression of tunneling.

PACS numbers: 73.23.-b, 85.65.+h, 73.63.Kv,

I. INTRODUCTION

Since its discovery in the late 50s by Anderson,¹ localization of the electronic wave function in a random medium became a paradigm of quantum coherence in condensed matter physics. In his seminal paper, Anderson proved that non-interacting electrons in three dimensions are spatially localized for sufficiently large disorder. Shortly after, Mott and Twose established that in one-dimension all the states of random systems become exponentially localized for any amount of disorder due to coherent backscattering.² Moreover, Abrahams *et al.*³ confirmed this statement by introducing a single-parameter scaling theory of localization and extended the Mott-Twose result to two-dimensional systems as well. With a few exceptions,⁴⁻⁷ the single-parameter scaling theory generally provides a very accurate picture of the electronic states in non-interacting disordered systems. In real solids, however, electrons interact with each other and with lattice vibrations, and these interactions are expected to have a strong impact on the transport properties of disordered systems. Since spatial localization of the electron wave function by disorder arises from an interference phenomenon, interactions often weaken localization. In this regard, Kopidakis *et al.* found that electron-phonon interaction may decrease the ability of electrons to form localized states.⁸

The advent of nanotechnology has brought with it a renewed attention on Anderson localization because both the dimensionality of the system and/or the interactions can be controlled to some extent. Flores *et al.* studied carbon nanotubes and showed the appearance of a strong Anderson localization regime. They found that the electrical resistance increases exponentially with the length of the nanotube,⁹ in agreement with the single-parameter scaling theory.³ These authors came to the conclusion

that the coherence length was much larger than the localization length. It is known that electron-phonon interaction, which can be relatively strong in molecular systems, is one of the most important factors limiting the coherence length.¹⁰ However, the interplay between Anderson localization and electron-lattice interactions in quantum confined systems remains relatively unexplored.

In this work we study the impact of the electron-vibron interaction and disorder on the transport properties of a molecular nanowire (MNW), using the Keldysh non-equilibrium Green's function formalism.¹¹ The MNW is regarded as a quasi-one-dimensional organic crystal of self-assembled molecules.¹² Specifically, we consider a MNW with the two ends connected to ideal leads and assume that the electrons interact with a vibrational degree of freedom localized at each molecule. Disorder in the electronic environment of each molecule can originate from interactions with a random environment of solute molecules and ions surrounding the MNW. Unlike Ref. 13, we propose a two-probe configuration to diminish the conductance fluctuations found in four-probe setups. It should be stressed that we neglect the lateral motion of electrons in the MNW. Grange has recently established that the drift velocity-voltage characteristics shows a transition from wide to narrow wires, displaying additional peaks due to resonances with optical phonons.¹⁴ Since we only deal with quasi-one-dimensional MNWs, this transition is beyond the scope of our work. We examine the spectral function as well as the electric and heat currents through the MNW, driven out of equilibrium by either an applied electric bias or temperature gradient. One of our main findings is the strong effect of disorder on the electron transport properties of the MNW when the electron-vibron interaction is taken into account. The enhancement of the localization can be traced back to the exponential suppression of tun-

neling. The tunnel energy is reduced with increasing temperature when the electron-vibron interaction is non-negligible. Consequently, the ratio between the magnitude of disorder and the tunnel energy becomes larger for higher temperatures, which can be viewed as an increase of the effective disorder. Notice that due to the zero-point motion, the tunneling energy is already significantly decreased at $T = 0$, leading to a stronger effective disorder even in absence of background temperature.

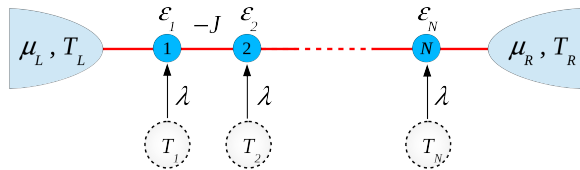


FIG. 1. (Color online) Schematic diagram of the MNW with intermolecular hopping energy J . The MNW is also connected to left and right leads. We take into account an intramolecular electron-vibron interaction, λ being the coupling constant and T_i the temperature of the bath for each molecule.

II. MODEL AND FORMALISM

We consider a MNW composed of N self-assembled molecules and connected to left (L) and right (R) leads by tunnel couplings, as shown schematically in Fig. 1. The chemical potentials of the leads under a bias voltage V are given by $\mu_L = \mu + eV/2$ and $\mu_R = \mu - eV/2$, where μ is the equilibrium chemical potential. Their temperatures are set as $T_L = T - \Delta T/2$ and $T_R = T + \Delta T/2$, where T is an average temperature and ΔT is the temperature difference between the hot and the cold leads.

Only one energy level in each molecule is assumed relevant and electron-electron interaction is neglected. On-site energies are subjected to disorder representing inhomogeneous broadening. Then, the energy level of the molecule i splits as $\varepsilon_i = \varepsilon + \Delta\varepsilon_i$, where $\Delta\varepsilon_i$ is a random uncorrelated variable whose distribution function is $P(\Delta\varepsilon_i) = 1/W$ if $|\Delta\varepsilon_i| < W/2$ and zero otherwise. W will be referred to as magnitude of disorder. In addition, the electron interacts with a local vibration mode (vibron) at each molecule which we assume of the same frequency ω_0 for simplicity. Besides the different temperature of the leads, we introduce a temperature gradient in the system by setting a different temperature T_i of each bath (see Fig. 1). In this work we interpolate linearly T_i between T_L and T_R .

A. The coupled electron-vibron system

The Hamiltonian describing the whole system splits into three contributions as $H = H_0 + H_{e\text{-leads}} +$

$H_{e\text{-vib}}$. The term H_0 describes the dynamics of the non-interacting system (we set $\hbar = 1$)

$$H_0 = \sum_{i=1}^N \varepsilon_i c_i^\dagger c_i - J \sum_{i=1}^{N-1} \left(c_i^\dagger c_{i+1} + c_{i+1}^\dagger c_i \right) + \omega_0 \sum_{i=1}^N a_i^\dagger a_i + \sum_{\alpha k} \varepsilon_{\alpha k} d_{\alpha k}^\dagger d_{\alpha k}. \quad (1)$$

Here $d_{\alpha k}^\dagger$ ($d_{\alpha k}$) denotes the creation (annihilation) operator of a conduction electron in the lead $\alpha = L, R$ with crystal momentum k and energy $\varepsilon_{\alpha k}$. Similarly, c_i^\dagger (c_i) is the creation (annihilation) operator of an electron in the molecule i with energy ε_i . J denotes the intermolecular hopping energy and it is assumed positive. Finally, the creation (annihilation) operator of a vibron in the molecule i with frequency ω_0 is denoted by a_i^\dagger (a_i).

The MNW is tunnel-coupled to both leads, as shown schematically in Fig 1. Therefore, the corresponding Hamiltonian reads

$$H_{e\text{-leads}} = \sum_{\alpha k i} \left(V_{\alpha k i} d_{\alpha k}^\dagger c_i + V_{\alpha k i}^* c_i^\dagger d_{\alpha k} \right). \quad (2)$$

We take a Holstein-type coupling between the electron and the vibrons¹⁵

$$H_{e\text{-vib}} = \lambda \sum_i \left(a_i^\dagger + a_i \right) c_i^\dagger c_i. \quad (3)$$

The electron-vibron coupling constant λ is assumed uniform over the chain.

We now apply the polaron (Lang-Firsov) nonperturbative canonical transformation $\tilde{H} = e^S H e^{-S}$, where the operator S is defined as $S = (\lambda/\omega_0) \sum_i (a_i^\dagger - a_i) c_i^\dagger c_i$.¹⁶ This transformation yields the following transformed Hamiltonian

$$\tilde{H} = \sum_{i=1}^N \tilde{\varepsilon}_i c_i^\dagger c_i - J \sum_{i=1}^{N-1} \left(X_i^\dagger X_{i+1} c_i^\dagger c_{i+1} + X_{i+1}^\dagger X_i c_{i+1}^\dagger c_i \right) + \omega_0 \sum_{i=1}^N a_i^\dagger a_i + \sum_{\alpha k i} \left(V_{\alpha k i} X_i d_{\alpha k}^\dagger c_i + V_{\alpha k i}^* X_i^\dagger c_i^\dagger d_{\alpha k} \right), \quad (4)$$

where $\tilde{\varepsilon}_i = \varepsilon_i - \lambda^2/\omega_0$ is the renormalized energy level of the molecule i . After the transformation, a new operator arises, $X_i = \exp[-(\lambda/\omega_0)(a_i^\dagger - a_i)]$, named the displacement operator. The canonical transformation is exact but it does not diagonalize the Hamiltonian. In other words, \tilde{H} still contains products of boson and fermion operators. When the coupling to the leads is weak ($|V_{\alpha k i}| \ll \lambda$), it is reasonable to replace the displacement operator X_i by its thermal expectation value evaluated in equilibrium $\langle X_i \rangle = \exp[-\xi_i(T_i)/2]$,^{17,18} where $\xi_i(T_i) = g(2n_i + 1)$ and $n_i = 1/[\exp(\omega_0/k_B T_i) - 1]$. The Huang-Rhys factor is given as $g = \lambda^2/\omega_0^2$. After

this replacement the transformed Hamiltonian is approximately given by

$$\begin{aligned} \tilde{H} \approx & \sum_{i=1}^N \tilde{\varepsilon}_i c_i^\dagger c_i - \sum_{i=1}^{N-1} \left(\tilde{J}_i c_i^\dagger c_{i+1} + \text{H.c.} \right) + \sum_{i=1}^N \omega_0 a_i^\dagger a_i \\ & + \sum_{\alpha ki} \left(\tilde{V}_{\alpha ki} d_{\alpha k}^\dagger c_i + \text{H.c.} \right), \end{aligned} \quad (5)$$

with $\tilde{J}_i = J \exp[-\xi_i(T_i)/2 - \xi_{i+1}(T_{i+1})/2]$ and $\tilde{V}_{\alpha ki} = V_{\alpha ki} \exp[-\xi_i(T_i)/2]$. Notice that the higher the temperature, the smaller the dressed couplings among the molecules and between them and the leads, as pictured in Fig. 2. This will be referred to as exponential suppression of tunneling.¹⁹ It is worth mentioning that $\tilde{J}_i/J < 1$ at $T = 0$ due to the zero-point motion.

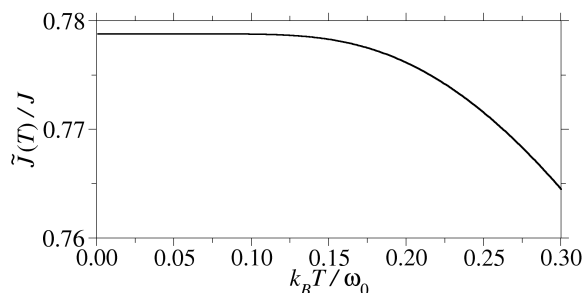


FIG. 2. Temperature dependence of the dressed hopping energy \tilde{J}_i among the molecules at an electron-vibron coupling strength of $\lambda = 0.25$, in units of the bare hopping energy J . In the absence of temperature gradient the dressed hopping energy is independent of the site index. The observed monotonic decay continues for larger T values.

B. Non-equilibrium Green's functions

Non-equilibrium transport properties of an interaction region coupled to two leads can be obtained with the help of the Keldysh non-equilibrium Green's function technique.²⁰ The various Green's functions of the system are lengthy but straightforward to calculate numerically. First, since we replaced the operator X_i by its thermal expectation value, the Green's functions are then factored out. The greater Green's function can be cast in the form

$$G_{ij}^>(t) = \tilde{G}_{ij}^>(t) \langle X_i(t) X_j^\dagger(0) \rangle, \quad (6)$$

where $\tilde{G}_{ij}^>(t)$ denotes the so called dressed greater Green's function. Concerning the vibron part, we may encounter two different cases. If $i \neq j$ then $\langle X_i(t) X_j^\dagger(0) \rangle = \exp[-\xi_i(T_i)/2 - \xi_j(T_j)/2]$. When $i = j$ the calculation is more involved and the final result is²¹

$$\langle X_i(t) X_i^\dagger(0) \rangle = \sum_{n=-\infty}^{\infty} L_n^i(T_i) e^{in\omega_0 t}, \quad (7a)$$

where at finite temperature

$$L_n^i(T_i) = e^{-\xi_i(T_i) + n\omega_0/2k_B T_i} I_n \left(\sqrt{\xi_i^2(T_i) - g^2} \right), \quad (7b)$$

with $I_n(z)$ the modified Bessel function of integer order, and at $T_i = 0$

$$L_n^i(0) = \begin{cases} e^{-g} g^n / n! & \text{if } n \geq 0, \\ 0 & \text{if } n < 0. \end{cases} \quad (7c)$$

The next step is the transformation into Fourier space and the calculation of the greater and lesser Green's functions to obtain the spectral matrix

$$A(\omega) = i[G^>(\omega) - G^<(\omega)], \quad (8)$$

along with the spectral function $A(\omega) = \text{Tr}[A(\omega)]/N$. Using the vibron mean values given above, the elements of the greater Green's functions are given as¹⁷

$$\begin{aligned} G_{ii}^>(\omega) &= \sum_{n=-\infty}^{\infty} L_n^i \tilde{G}_{ii}^>(\omega - \omega_0 n), \\ G_{ij}^>(\omega) &= \langle X_i \rangle \langle X_j \rangle \tilde{G}_{ij}^>(\omega), \quad i \neq j, \end{aligned} \quad (9)$$

and similarly for the lesser Green's function but replacing $\omega - \omega_0 n$ by $\omega + \omega_0 n$ in the summation. The dressed lesser and greater Green's functions can be calculated from the Keldysh equation $\tilde{G}^{<(>)}(\omega) = \tilde{G}^r(\omega) \tilde{\Sigma}^{<(>)}(\omega) \tilde{G}^a(\omega)$, where the self-energies are given by

$$\begin{aligned} \tilde{\Sigma}^<(\omega) &= i \left[f_L^{(e)}(\omega) \tilde{\Gamma}^L + f_R^{(e)}(\omega) \tilde{\Gamma}^R \right], \\ \tilde{\Sigma}^>(\omega) &= -i \left[f_L^{(h)}(\omega) \tilde{\Gamma}^L + f_R^{(h)}(\omega) \tilde{\Gamma}^R \right], \end{aligned} \quad (10)$$

with $f_\alpha^{(e)}(\omega) = f_\alpha(\omega)$ and $f_\alpha^{(h)}(\omega) = 1 - f_\alpha(\omega)$. Here $f_\alpha(\omega) = 1 / \{ \exp[(\omega - \mu_\alpha)/k_B T_\alpha] + 1 \}$ is the Fermi-Dirac distribution function of the lead α . The matrix elements of $\tilde{\Gamma}^\alpha$ in (10) are given as $\tilde{\Gamma}_{ij}^\alpha = 2\pi \rho_\alpha \tilde{V}_{\alpha ki} \tilde{V}_{\alpha kj}^*$, where ρ_α is the density of states of the corresponding lead. Notice that we will neglect their k -dependence by relying on the wide-band limit approximation and take $\tilde{\Gamma}^\alpha$ matrices as energy-independent magnitudes.

C. Electric and heat currents

In order to calculate the dressed retarded Green's function, the equation-of-motion method is used. It is straightforward to show that

$$\begin{aligned} (\omega - \tilde{\varepsilon}_i) \tilde{G}_{ij}^r(\omega) &= \delta_{ij} - \tilde{J}_i \tilde{G}_{i+1,j}^r(\omega) - \tilde{J}_{i-1} \tilde{G}_{i-1,j}^r(\omega) \\ &+ \sum_{l=1}^N \tilde{\Sigma}_{il}^r \tilde{G}_{lj}^r(\omega), \end{aligned} \quad (11)$$

where

$$\tilde{\Sigma}_{il}^r = \sum_{\alpha k} \frac{\tilde{V}_{\alpha ki}^* \tilde{V}_{\alpha kl}}{\omega - \varepsilon_{\alpha,k} + i0^+} \quad (12a)$$

is the retarded self-energy. Within the wide-band approximation this term is written as

$$\tilde{\Sigma}_{il}^r(\omega) = \frac{i}{2} \langle X_i \rangle \langle X_l \rangle (\Gamma_{il}^L + \Gamma_{il}^R). \quad (12b)$$

Similarly, the advanced self-energy is given as

$$\tilde{\Sigma}_{il}^a(\omega) = -\frac{i}{2} \langle X_i \rangle \langle X_l \rangle (\Gamma_{il}^L + \Gamma_{il}^R). \quad (12c)$$

Once the dressed Green's functions are known, we can obtain the spectral matrix (8) using (9). In addition, we can also calculate the symmetrized electric current¹¹

$$J_e = \frac{e}{2} \int \frac{d\omega}{2\pi} \text{Tr} \left[(\Gamma^L - \Gamma^R) iG^< + (f_L(\omega)\Gamma^L - f_R(\omega)\Gamma^R) \mathcal{A}(\omega) \right]. \quad (13a)$$

Unlike the electric current, the heat current is not necessarily conserved due to the coupling to the heat baths and Joule heating. We will mainly concentrate on the heat current from the left lead to the MNW

$$J_Q^L = \int \frac{d\omega}{2\pi} \omega \text{Tr} \left[\Gamma^L iG^<(\omega) + f_L(\omega)\Gamma^L \mathcal{A}(\omega) \right] - \mu_L \frac{J_e}{e}, \quad (13b)$$

which is expected to differ from the heat current J_Q^R from the right lead to the MNW. In the following sections the electric and heat currents will be expressed in units of $e\omega_0/2\pi$ and $\omega_0^2/2\pi$, respectively. The superscript L in (13b) will be removed unless stated otherwise.

III. SPECTRAL FUNCTION

In this section we present and discuss the salient features of the spectral function $A(\omega)$. For concreteness we restrict ourselves to the equilibrium regime by setting $\mu_L = \mu_R = 0$ and $\Delta T = 0$ throughout this section. To gain insight into the effect of the electron-vibron interaction we compare the numerically calculated spectral density in the non-interacting MNW ($\lambda = 0$) with a wire where the electron-vibron coupling strength is finite ($\lambda = 0.5$). Energies are expressed in units of the vibron energy ω_0 in what follows (recall that we set $\hbar = 1$). To have a clear picture, the coupling to the leads is taken as symmetric with $\Gamma_{1,1}^L = \Gamma_{N,N}^R = 0.2$ ($\Gamma_{ij}^\alpha = 0$ otherwise), the bare intermolecular hopping energy is $J = 0.1$ and $N = 20$.

Figure 3(a) shows the spectral density of a uniform MNW ($W = 0$) with constant on-site energy $\varepsilon_0 = 0.25$ (blue solid line) and $\varepsilon_0 = 0$ (red solid line), which corresponds to renormalized energies $\tilde{\varepsilon}_0 = 0$ and $\tilde{\varepsilon}_0 = -0.25$ when $\lambda = 0.5$, respectively. The temperature of the system is $k_B T = 0.1$. Results are compared to the non-interacting case ($\lambda = 0$, black dashed line) when $\varepsilon_0 = 0$, whose spectral density displays the expected U -shaped

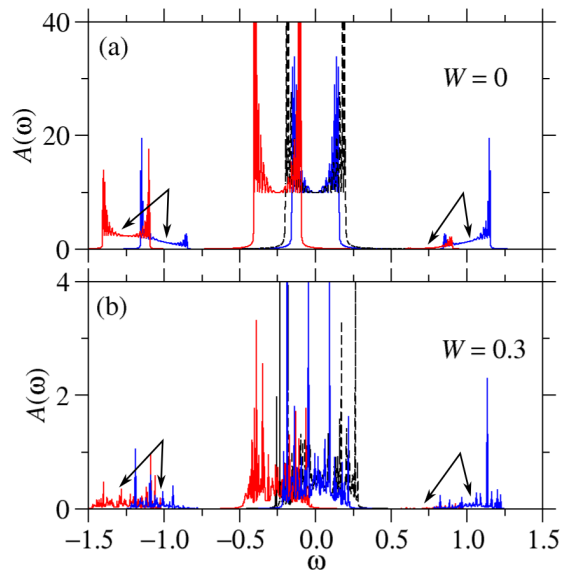


FIG. 3. (Color online) Spectral function at $k_B T = 0.1$ for a MNW symmetrically coupled to leads ($\Gamma_L = \Gamma_R = 0.2$) with (a) no disorder and (b) random on-site energies ($W = 0.3$), averaged over 100 realizations. The number of molecules is $N = 20$. Blue and red solid lines correspond to finite electron-vibron coupling ($\lambda = 0.5$) when $\varepsilon_0 = 0.25$ and $\varepsilon_0 = 0$, respectively. Black dashed lines show the spectral density of the non-interacting wire ($\lambda = 0$) when $\varepsilon_0 = 0$. For clarity, the error bars of the averages in panel (b) are not shown. The arrows in panels (a) and (b) point at the first-order side bands of the interacting systems.

profile of width $4\tilde{J}$ corresponding to a one-dimensional lattice with dressed intermolecular hopping energy \tilde{J} . When the electron-vibron interaction is turned on (red solid line), the zero-vibron band of the spectral density is red-shifted with regard to the non-interacting case, according to the renormalization of the on-site energy $\tilde{\varepsilon}_0 = \varepsilon_0 - \lambda^2 = -0.25$ associated to the deformation of the lattice around the tunneling electron.²² Furthermore, the finite electron-vibron interaction leads to the formation of side bands centred at energies $\tilde{\varepsilon}_0 - 1$ and $\tilde{\varepsilon}_0 + 1$, which correspond to emission or absorption of vibrational energy, respectively. As the thermal energy is small compared to the vibrational energy ($k_B T \ll \omega_0$), the latter contribution is weak, which leads to an asymmetric spectral density $A(\omega)$ and therefore to a broken particle-hole symmetry in the case $\tilde{\varepsilon}_0 \neq 0$. For the case of a renormalized energy of $\tilde{\varepsilon}_0 = 0$ (blue solid line), the particle-hole symmetry is established and the side bands are symmetric. It has to be noted that the sum rule $\int d\omega \mathcal{A}(\omega) = 2\pi$ still holds, so that the additional contribution due to the side channels are compensated by decreasing the height of the zero-vibron band with respect to the non-interacting case, as seen when comparing the blue solid line with the black dashed line.¹⁷

In summary, the effect of the electron-vibron interaction on the spectral density of a uniform MNW is similar

to the case of a single molecule.¹⁷ The most significant difference is the level splitting to form a band due to the intermolecular coupling and the resulting narrowing arising from the renormalization of the intermolecular hopping energy \tilde{J} with respect to the non-interacting case J .

We now introduce strong disorder with magnitude $W = 0.3$, which is of the order of the MNWs bandwidth. Figure 3(b) shows the resulting spectral function when the other parameters are the same as in Fig. 3(a). The displayed values were calculated by averaging over 100 realizations. As expected, the obtained spectral densities show a much more complicated structure but the sum-rule $\int A(\omega)d\omega = 2\pi$ remains valid, as the distribution of levels becomes random after introducing disorder. The effect of the electron-vibron interaction on the spectral function does not seem to differ much from the case without disorder. In particular, no midgap channels induced by disorder were found, in contrast to short molecular systems with a single defect.²³

IV. VOLTAGE-DRIVEN ELECTRIC TRANSPORT

We now turn to the impact of the electron-vibron interaction on the electric response of the MNW out of equilibrium. To this end, we calculate the non-linear dependence of the electric current given by Eq. (13a) on the source-drain voltage V . As the charge transport across the wire is strongly dominated by resonant tunneling processes, the electric current and the differential conductance $\mathcal{G}(V, \Delta T = 0) = dJ_e/dV|_{\Delta T=0}$ give a good insight into the complex non-linear transmission function of the system. We also calculate the heat current J_Q from Eq. (13b). We first discuss the simpler case of the MNW without disorder ($W = 0$) and later compare it to the electric response of the system subjected to disorder ($W = 0.3$). In both cases the electric response is computed for a MNW with ($\lambda = 0.5$) and without ($\lambda = 0$) electron-vibron interaction. The rest of parameters are the same as in Fig. 3.

A. Uniform molecular nanowires

Figure 4 shows the non-linear conductance at (a) a low temperature of $k_B T = 0.01$ and (b) an intermediate temperature of $k_B T = 0.2$ as a function of eV for a MNW without disorder. The general shape of the low temperature conductance of the different cases in Fig. 4 follows the general trends of the spectral function shown in Fig. 3(a). This can be easily explained by the close relation between the conductance and the electronic transmission properties through the chain, with peaks corresponding to the resonant transmission channels shown by the spectral function. Notice the smearing out of the conductance due to the finite temperature and the symmetry

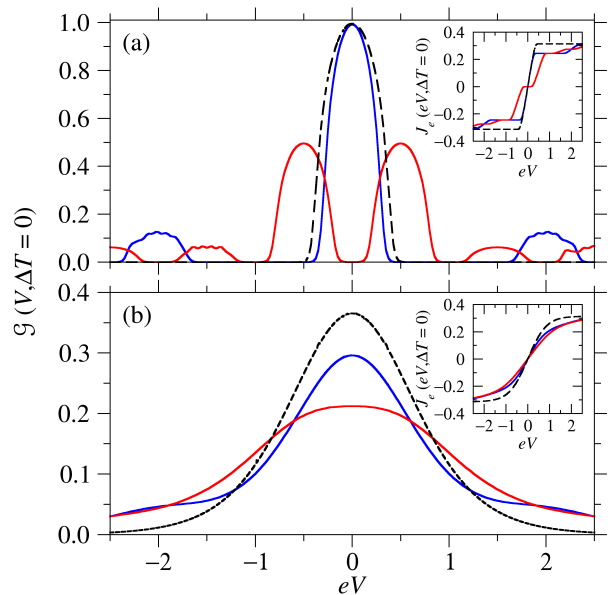


FIG. 4. (Color online) Differential electric conductance as a function of eV for a MNW without disorder at (a) $k_B T = 0.01$ and (b) $k_B T = 0.2$. Blue and red solid lines correspond to finite electron-vibron coupling ($\lambda = 0.5$) when $\varepsilon_0 = 0.25$ and $\varepsilon_0 = 0$. Black dashed lines show the results for the non-interacting MNW ($\lambda = 0$) when $\varepsilon_0 = 0$. The insets show the corresponding electric currents.

of $\mathcal{G}(V, \Delta T = 0)$ and $J_e(eV, \Delta T = 0)$ against eV . This is due to the upward and downward shift of the chemical potential of the left ($+eV/2$) and right ($-eV/2$) leads produced by the applied bias. Thus, a finite contribution of $\mathcal{G}(V, \Delta T = 0)$ will correspond to energies $\omega = \pm eV/2$ where the spectral density is non-zero.

In the case without electron-vibron interaction shown in Fig. 4(a) (black dashed line), the conductance in the uniform MNW only exhibits finite values within the band, as expected. For systems with finite electron-vibron interaction ($\lambda = 0.5$) the differential electric conductance of a MNW with a renormalized on-site energy $\tilde{\varepsilon}_0 = 0$ (blue solid line) resembles the case without interaction, with a maximum at $eV = 0$ corresponding to the zero-vibron peak. The width of the peak is narrower due to the reduced hopping energy $\tilde{J} < J$. On the other hand, the differential conductance also shows additional side peaks at about $eV = \pm 2$, i.e., $\omega = \pm 1$, which match the transmission channels created by the absorption and emission of vibrons. When the renormalized on-site energy is nonzero (see red solid line, corresponding to $\tilde{\varepsilon}_0 = -0.25$), the central maximum disappears and two zero-vibron peaks at $eV = \pm 0.5$ arise instead. This is due to the fact that transmissions channels are open only for either holes or electrons but not for both simultaneously. In addition, the red solid line shows two more side peaks at $eV = \pm 1.5$ and $eV = \pm 2.5$, the former matching the transmission channel at $\tilde{\varepsilon}_0 + 1 = 0.75$ and the latter $\tilde{\varepsilon}_0 - 1 = -1.25$. Interestingly, the weight of the local

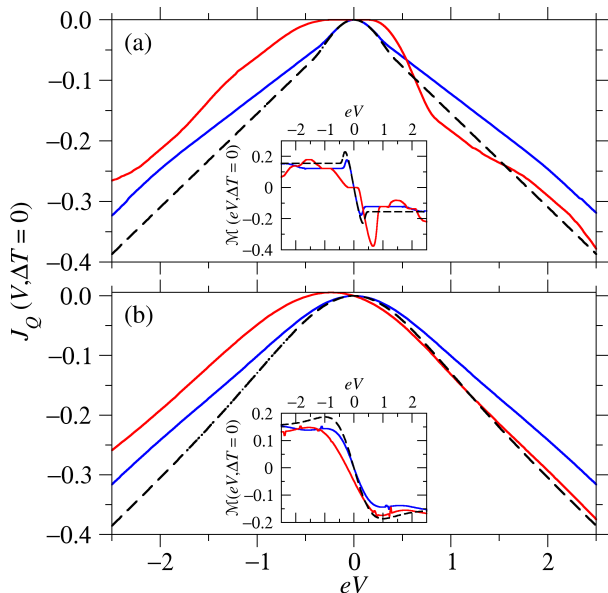


FIG. 5. (Color online) Heat current as a function of eV for MNWs without disorder as in the case of Fig. 4 at (a) $k_B T = 0.01$ and (b) $k_B T = 0.2$. Blue and red solid lines correspond to finite electron-vibron coupling ($\lambda = 0.5$) when $\varepsilon_0 = 0.25$ and $\varepsilon_0 = 0$. Black dashed lines show the results for the non-interacting wire ($\lambda = 0$) when $\varepsilon_0 = 0$. The insets display the corresponding differential electrothermal conductance $\mathcal{M}(V, \Delta T = 0) = dJ_Q/dV|_{\Delta T=0}$.

maxima at $eV = \pm 1.5$ is very large in comparison to the spectral function depicted in Fig. 3. The inset in Fig. 4(a) shows the electric current $J_e(V, \Delta T = 0)$ corresponding to the conductance of the main panel. $J_e(V, \Delta T = 0)$ clearly displays the same saturation value independent of λ , which indicates that we do not induce any real scattering with the electron-vibron interaction and which corresponds to the conservation of the spectral sum-rule discussed in Sec. III. Figure 4(b) displays the conductance at a higher temperature $k_B T = 0.2$. The different local maxima seen in Fig. 4(a) reduce to a single wide peak due to the thermal smearing out of the Fermi-Dirac distribution in the leads. Also here the saturation values of the electric current with and without electron-vibron interaction are the same.

Figure 5 shows the heat current $J_Q(V)$ as a function of eV at (a) low $k_B T = 0.01$ and (b) intermediate $k_B T = 0.2$ temperatures for the same cases shown in Fig. 4. Unlike the electric current, the heat current does not saturate at high eV due to Joule heating. The observed linear behavior of $J_Q(V, \Delta T = 0)$ at high voltage manifests itself in the saturation of the differential electrothermal conductance $\mathcal{M}(V, \Delta T = 0) = dJ_Q/dV|_{\Delta T=0}$ (shown in the insets). The electron transmission properties can be depicted in the non-linear progression of the differential electrothermal conductance \mathcal{M} , where we see strong deviations compared to the differential electric conductance \mathcal{G} due to the Joule heating $\mu_L J_e/e$

and the weighting by the tunneling electron energy ω in Eq. (13b). One should note the strong resemblance of the $J_Q(V, \Delta T = 0)$ curves without electron-vibron interaction (black dashed lines) and the corresponding curve with the coupling switched on for the same bare on-site energy $\varepsilon_0 = 0$ (red solid lines) for $eV > 0$. This can be explained by the small contribution of thermally generated vibrons at low background temperatures, so that the total energy is nearly conserved when switching on the electron-vibron interaction. Therefore, when the electric bias is high enough and all vibronic side bands are open for transmission, the total energy transferred to the system is approximately conserved after switching on the interaction. On the contrary, this conservation does not hold for an electric bias such $eV < 0$ due to the breaking of the electron-hole symmetry (asymmetry of the transmission about $\omega = 0$) by switching on the interaction, as discussed in the previous section. Unlike the symmetric electric current $J_e(V)$, this asymmetric transmission can be seen in the heat current from the left lead to the MNW (13b). On the other hand, the blue solid lines, which correspond to a renormalized on-site energy $\tilde{\varepsilon}_0 = 0$ and therefore a symmetric transmission, also shows a heat current symmetric about $eV = 0$.

B. Disordered molecular nanowires

Figure 6(a) shows the differential electric conductance $\mathcal{G}(V, \Delta T = 0)$ of disordered MNWs with $W = 0.3$ at $k_B T = 0.01$, averaged over 100 realizations, and the other parameters as in Fig. 4. The main features of the curves resemble those without disorder, the main difference being the occurrence of sharper peaks and a strong reduction of the maximum differential electric conductance. The conductance is reduced by a factor of ~ 8 for the chain without electron-vibron interaction, and up to ~ 15 for the interacting case. When temperature is increased up to $k_B T = 0.2$ the peaks of the differential conductance become broader and even merge into a single one in the case $\lambda = 0.5$ and $\varepsilon_0 = 0$ (not shown) as for the ordered MNW in Fig. 4(b).

In addition, the differential electric conductance is further decreased if the length of the MNW increases from $N = 20$ to $N = 40$, as displayed in Fig. 6(b). This behavior is in contrast to the uniform MNW, where the conductance is preserved against the system length. It is worth noting the stronger reduction in the MNW with finite electron-vibron interaction when doubling the length, compared to the case without interaction. Such a reduction can be traced back to the Anderson-localization of electron states.¹⁻³ In general, the magnitude of disorder has to be compared with the hopping energy or, in other words, with the bandwidth of the uniform system. The larger the ratio between them, the smaller the localization length. From this reasoning, the effects of disorder should be more important on increasing temperature when the electron-vibron coupling is finite since the expo-

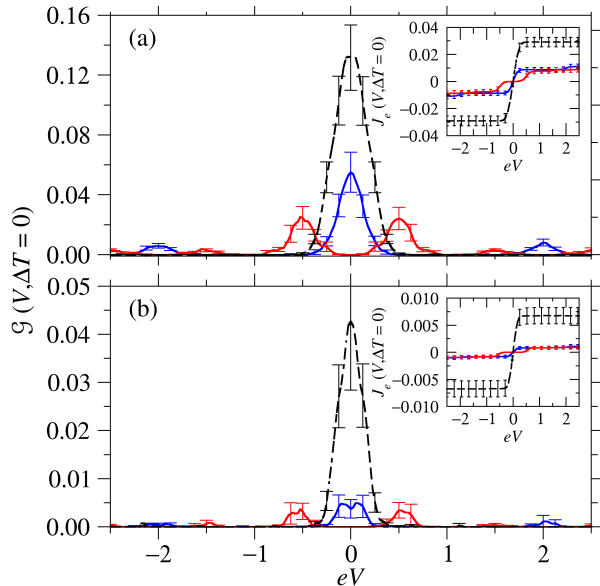


FIG. 6. (Color online) Differential electric conductance at $k_B T = 0.01$ as a function of eV of MNWs of length (a) $N = 20$ and (b) $N = 40$ subjected to disorder ($W = 0.3$). Results were averaged over 100 realizations. The other parameters are the same as in Fig. 4. Blue and red solid lines correspond to finite electron-vibron coupling ($\lambda = 0.5$) when $\varepsilon_0 = 0.25$ and $\varepsilon_0 = 0$. Black dashed lines show the results for the non-interacting wire ($\lambda = 0$) when $\varepsilon_0 = 0$. The inset shows the corresponding electric current.

nential suppression of tunneling reduces the dressed intermolecular hopping energy \tilde{J} . The expected reduction of the localization length is hinted from the comparison of Figs. 4 and 6.

For completeness, Fig. 7 shows the the heat current $J_Q(V, \Delta T)$ in disordered MNWs with $W = 0.3$ and the rest of parameters as in Fig. 5. The influence of disorder agrees well with the observed electric current, supporting the idea of an increased localization in the case of finite electron-vibron interaction that influences both charge and heat transport alike.

V. TEMPERATURE-DRIVEN ELECTRIC TRANSPORT

We now investigate the electric transport through MNWs in response to a temperature difference ΔT only. We are assuming a symmetrically biased system with $T_L = T - \Delta T/2$ and $T_R = T + \Delta T/2$, therefore keeping the average temperature $(T_L + T_R)/2$ at a defined value T . In order to ensure that each site-dependent $T_i > 0$, the maximum ΔT_{\max} is fixed at $\Delta T_{\max} = \pm T/2$ so that the leads do not deviate more than 25 % from their initial temperature. In this section, the bias voltage is absent ($V = 0$) and charge flows through the MNW only due to the temperature difference between the leads. As in

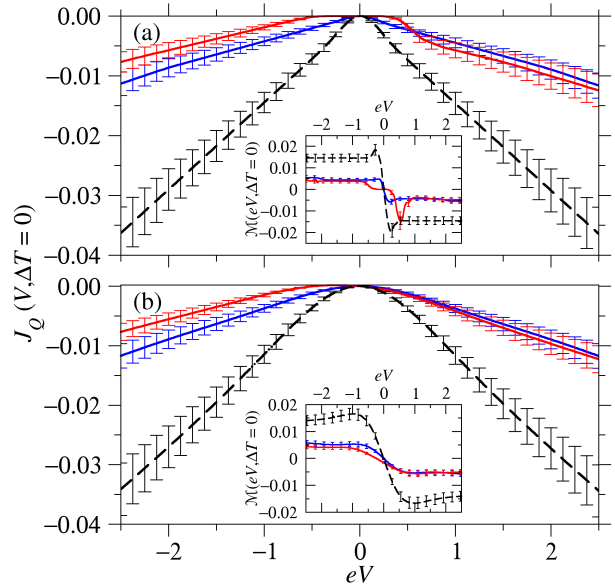


FIG. 7. (Color online) Heat current as a function of eV of MNWs with disorder ($W = 0.3$) averaged over 100 realizations at (a) $k_B T = 0.01$ and (b) $k_B T = 0.2$. The other parameters are the same as in Fig. 5. Blue and red solid lines correspond to finite electron-vibron coupling ($\lambda = 0.5$) when $\varepsilon_0 = 0.25$ and $\varepsilon_0 = 0$. Black dashed lines show the results for the non-interacting wire ($\lambda = 0$) when $\varepsilon_0 = 0$. The insets show the corresponding differential electrothermal conductance.

Sec. IV we first discuss the electric and heat currents in uniform MNWs ($W = 0$) and later we consider random on-site energies with $W = 0.3$. The other parameters of the system are taken the same as in Sec. IV, with the additional case of a non-interacting MNW with on-site energy $\varepsilon_0 = 0.25$.

A. Uniform molecular nanowires

Figure 8(a) shows the electric current $J_e(V = 0, \Delta T)$ at $k_B T = 0.2$ as a function of ΔT for a MNW without disorder. The blue solid line ($\lambda = 0.5$ and $\tilde{\varepsilon}_0 = 0$) and the black dashed line ($\lambda = 0$ and $\varepsilon_0 = 0$), which represent systems with symmetric transmission around the Fermi energy $\mu_L = \mu_R = 0$, do not exhibit any thermoelectric current at all. This is due to the fact that, in case of a thermal bias, all electrons tunneling from the hot lead to the unoccupied states of the cold lead are compensated by holes tunneling from the unoccupied states to the still occupied state of the cold lead due to the electron-hole symmetry. If this symmetry is broken, as in the case of the red solid line ($\lambda = 0.5$ and $\tilde{\varepsilon}_0 = -0.25$) and the blue dotted line ($\lambda = 0$ and $\varepsilon_0 = 0.25$), the system exhibits a finite thermally-driven electron or hole currents. Unlike the voltage-driven case, this current is nearly linear since the temperature difference is not high enough to reach a non-linear regime.

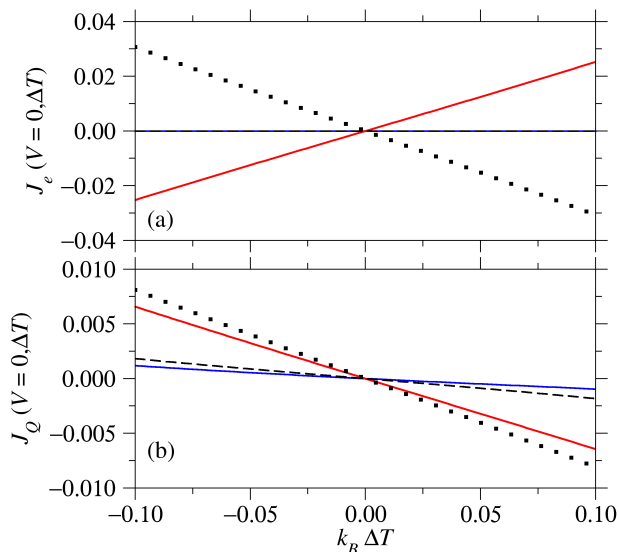


FIG. 8. (Color online) Temperature-driven (a) electric current J_e and (b) heat current J_Q as a function of the temperature difference ΔT for MNWs without disorder ($W = 0$) at $k_B T = 0.2$. Blue and red solid lines correspond to finite electron-vibron coupling ($\lambda = 0.5$) when $\varepsilon_0 = 0.25$ and $\varepsilon_0 = 0$. Black dashed (superimposed on the blue solid line) and dotted lines show the results for the non-interacting wire ($\lambda = 0$) when $\varepsilon_0 = 0$ and $\varepsilon_0 = 0.25$, respectively.

Figure 8(b) displays the heat current $J_Q(V = 0, \Delta T)$ at $k_B T = 0.2$ as a function of ΔT . Unlike the electric current $J_e(V = 0, \Delta T)$, also the blue solid line ($\lambda = 0.5$ and $\tilde{\varepsilon}_0 = 0$) and the black dashed line ($\lambda = 0$ and $\varepsilon_0 = 0$) exhibit finite values due to weighting of the tunneling particles with their respective energies and the asymmetry of the heat currents from the left and the right leads ($J_Q^L \neq J_Q^R$). As the majority of the carriers are transmitted through the zero-vibron channel, the transmitted energy and therefore the heat current is rather low compared to the other two cases, whose main transmission channels are centered at a finite energy. A small influence of the electron-vibron interaction can be seen as a slight asymmetry of the absolute value of the thermal current $|J_Q(\Delta T)| \neq |J_Q(-\Delta T)|$ for the cases with finite λ . Such an effect can also be depicted for disordered MNWs in the next section and it shall be discussed on that behalf.

B. Disordered molecular nanowires

Figure 9(a) shows the average temperature-driven electric current $J_e(V = 0, \Delta T)$ as a function of the temperature difference ΔT for the same systems shown in Fig. 8 but with disorder of magnitude $W = 0.3$. As in the case of voltage-driven transport discussed in Sec. IV, disorder strongly alters the electric response of the MNW. We observe that it affects the interacting MNW more significantly than the non-interacting one. This can be

explained by the same reasoning introduced in Sec. IV.

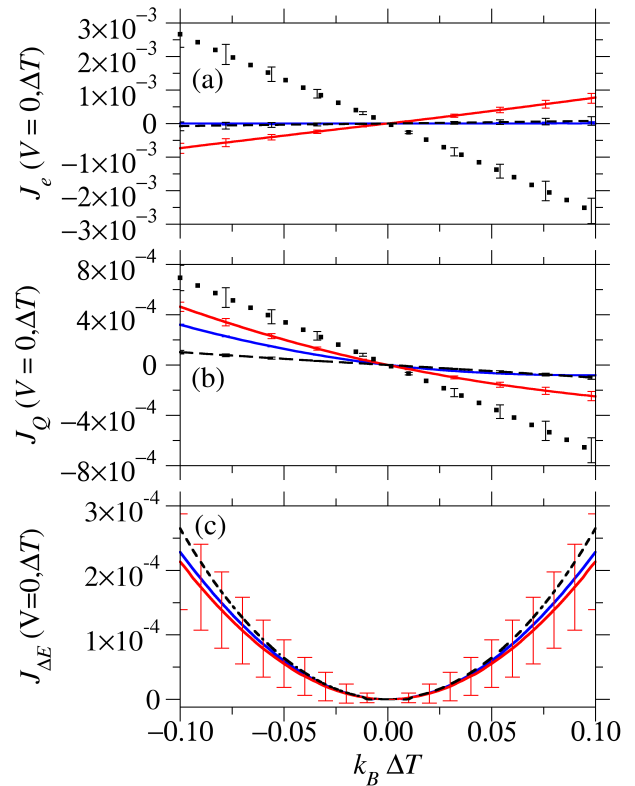


FIG. 9. (Color online) Temperature-driven (a) electric current J_e and (b) heat current J_Q as a function of the temperature difference ΔT for MNWs with disorder ($W = 0.3$) at $k_B T = 0.2$. Blue and red solid lines correspond to finite electron-vibron coupling ($\lambda = 0.5$) when $\varepsilon_0 = 0.25$ and $\varepsilon_0 = 0$. Black dashed and dotted lines show the results for the non-interacting wire ($\lambda = 0$) when $\varepsilon_0 = 0$ and $\varepsilon_0 = 0.25$, respectively. Panel (c) displays the heat generation inside the MNW as a function of ΔT at $k_B T = 0.2$ for an $\varepsilon_0 = 0.25$ in the case without disorder (blue solid line) and with disorder (red solid line) calculated from Fig. 8(b) and 9(b) respectively. The black dashed line represents the occupation number of thermally generated vibrons times the thermoelectric current in arbitrary units as a function of ΔT .

Figure 9(b) displays the temperature-driven heat current $J_Q(V = 0, \Delta T)$ for the same parameters as in Fig. 9(a). One can see a strong non-linear curve progression for MNWs with finite coupling. More importantly, the interacting system actually exhibits a stronger or nearly equal heat current in comparison with the non-interacting one, at least for $\Delta T < 0$. As can be concluded from the effect of disorder seen in the electric current in Fig. 9(a), this can not be related to the electric response of the system. Therefore, it must arise from the heat transport properties. Due to the symmetry of the system at $\Delta T = 0$, the heat current $J_Q^L(-\Delta T)$ from the left lead to the systems according to Eq. (13b) at $-\Delta T$ is equal to the energy flux $J_Q^R(\Delta T)$ from the right lead to the system at ΔT . Following the reasoning

from Ref. 24 the sum $J_{\Delta E}(\Delta T) \equiv J_Q^L(\Delta T) + J_Q^R(\Delta T) = J_Q^L(\Delta T) + J_Q^L(-\Delta T)$ equals the rate of energy generated inside the MNW. Thus, the asymmetry between the $J_Q^L(-\Delta T)$ and $J_Q^L(\Delta T)$ must be explained by a heat generation process inside the system. As this heat generation process is only noticeable in interacting MNWs, it is reasonable to assume that it is due to the thermal generation of vibrons. At $k_B T = 0.2$ the amount of thermally generated vibrons is very small, which is why the asymmetry is much less visible in case of no disorder in Fig. 8(b) due to an order of magnitude higher overall $J_Q^L(\Delta T)$. But when actually calculating the heat generation rate $J_{\Delta E}$, as depicted in Fig. 9(c) for the case of $\varepsilon_0 = 0$, in good approximation one gets the same values for the ordered (magenta curve) and the disordered (red curve) MNW. This supports the explanation of an effect governed by the vibronic subsystem. In addition, the effect of heat generation gets further support when looking at the green curve in Fig. 9(c), which represents the total density of thermally generated vibrons inside the system times the electric current (to roughly amount for the number of electrons in the system to which the vibrons can couple), in arbitrary units. As the green curve clearly is proportional to the heat generation rate $J_{\Delta E}$, one can safely conclude that the additional heat is transferred from the heat baths to the MNW.

VI. CONCLUSIONS

In conclusion, we have studied the non-equilibrium transport properties of a disordered MNW. The wire is regarded as a quasi-one-dimensional organic crystal of random single-level molecules, connected in series to two leads. We also have assumed that the electron interacts with local vibrational modes in the molecules and investigated the effects of the interaction on the electric and heat currents in response to either an applied electric bias or temperature gradient established in the system. The polaron (Lang-Firsov) transformation and the subsequent replacement of the operators X_i by their expectation values $\langle X_i \rangle$ turns the original many-body problem into an effective one-body problem.

We have considered the regime of strong disorder, for which the localization length in the non-interacting MNW ($\lambda = 0$) is smaller than its length. In addition, we have taken $k_B T \ll \omega_0$ in our simulations and con-

sequently the scattering is mainly dominated by the interaction with the disordered lattice. This is supported by the fact that the voltage-driven electric current J_e in uniform MNWs ($W = 0$) is independent of the system length and its saturation value is the same for both non-interacting and interacting cases. Remarkably, we have found that the electron-vibron interaction enhances the effects of the disorder on the electric and heat currents. This important result can be understood as follows. The intermolecular hopping energy \tilde{J}_i in the interacting MNW is smaller than the bare one J due to the occurrence of the exponential suppression of tunneling.¹⁹ Therefore, disorder is effectively stronger when the interaction is switched on because the ratio between the magnitude of disorder and the bandwidth increases.

Regarding the temperature-driven transport, we have numerically found an almost linear dependence of the electric and heat currents on the temperature difference. In MNWs with preserved electron-hole symmetry the electric current vanishes even if the electron-vibron interaction is taken into account. On the contrary, the heat current is always non-zero and enhanced due to the interaction, although to a small extent. Most importantly, the effects of disorder are more pronounced in the interacting MNW.

In this work we concentrated our study to MNWs but our results can be extended to arrays of quantum dots as well. These arrays can be realized in electron gases with superposed mesh gates. Beside their interest in fundamental research, they are regarded as good candidates for building quantum simulators.²⁵⁻²⁷ Unavoidable imperfections introduced during the fabrication process might have an impact on charge and energy transport when electrons are coupled to bosonic degrees of freedom. Our results shed light on the influence of disorder on the performance of quantum simulators based on arrays of quantum dots.

ACKNOWLEDGMENTS

The authors are grateful to D. Sánchez, M. A. Sierra and C. Álvarez for helpful discussions. F. D-A. thanks the Theoretical Physics Group of the University of Warwick for the warm hospitality. Work at Madrid has been supported by MINECO under Grant MAT2013-46308. UK research data statement: All data accompanying this publication are directly available within the publication.

* elenadg@fis.ucm.es

¹ P. W. Anderson, Phys. Rev. **109**, 1492 (1958).

² N. F. Mott and W. D. Twose, Adv. Phys. **10**, 107 (1961).

³ E. Abrahams, P. W. Anderson, D. C. Licciardello, and T. V. Ramakrishnan, Phys. Rev. Lett. **42**, 673 (1979).

⁴ V. Bellani, E. Diez, R. Hey, L. Toni, L. Tarricone, G. B. Parravicini, F. Domínguez-Adame, and R. Gómez-Alcalá,

Phys. Rev. Lett. **82**, 2159 (1999).

⁵ A. Rodríguez, V. A. Malyshev, and F. Domínguez-Adame, J. Phys. A: Math. Gen. **33**, L161 (2000).

⁶ S. L. A. de Queiroz, Phys. Rev. B **66**, 195113 (2002).

⁷ A. Rodríguez, A. Chakrabarti, and R. A. Römer, Phys. Rev. B **86**, 085119 (2012).

- ⁸ G. Kopidakis, C. M. Soukoulis, and E. N. Economou, EPL (Europhysics Letters) **33**, 459 (1996).
- ⁹ F. Flores, B. Biel, A. Rubio, F. J. García-Vidal, C. Gómez-Navarro, P. de Pablo, and J. Gómez-Herrero, J. Phys.: Condens. Mat. **20**, 304211 (2008).
- ¹⁰ S. Datta, *Electronic Transport in Mesoscopic Systems* (Cambridge University Press, 1995).
- ¹¹ H. Haug and A. P. Jauho, *Quantum Kinetics in Transport and Optics of Semiconductors* (Springer, Berlin, 2007).
- ¹² Y. Wang, J. Zhou, and R. Yang, J. Phys. Chem. C **115**, 24418 (2011).
- ¹³ J. L. D'Amato and H. M. Pastawski, Phys. Rev. B **41**, 7411 (1990).
- ¹⁴ T. Grange, Phys. Rev. B **89**, 165310 (2014).
- ¹⁵ T. Holstein, Ann. Phys. **8**, 325 (1959).
- ¹⁶ I. G. Lang and Y. A. Firsov, Sov. Phys. JETP **16**, 1301 (1963).
- ¹⁷ Z.-Z. Chen, R. Lü, and B. Zhu, Phys. Rev. B **71**, 165324 (2005).
- ¹⁸ B. H. Wu, J. C. Cao, and C. Timm, Phys. Rev. B **86**, 035406 (2012).
- ¹⁹ W. Rudziński, J. Phys.: Condens. Mat. **20**, 275214 (2008).
- ²⁰ L. V. Keldysh, Sov. Phys. JETP **20**, 1018 (1965).
- ²¹ G. D. Mahan, *Many-Particle Physics* (Kluwer Academic, New York, 2000).
- ²² N. S. Wingreen, K. W. Jacobsen, and J. W. Wilkins, Phys. Rev. Lett. **61**, 1396 (1988).
- ²³ D. Nozaki, H. M. Pastawski, and G. Cuniberti, New J. Phys. **12**, 063004 (2010).
- ²⁴ M. Galperin, A. Nitzan, and M. A. Ratner, Phys. Rev. B **75**, 155312 (2007).
- ²⁵ I. Buluta and F. Nori, Science **326**, 108 (2009).
- ²⁶ S. J. Chorley, C. G. Smith, F. Pérez-Martínez, J. Prance, P. Atkinson, D. A. Ritchie, and G. A. C. Jones, Microelectron. J. **39**, 314 (2008).
- ²⁷ J. Gray, A. Bayat, R. K. Puddy, C. G. Smith, and S. Bose, Phys. Rev. B **94**, 195136 (2016).